RSC Advances

PAPER

View Article Online
View Journal | View Issue

Cite this: *RSC Adv.*, 2024, **14**, 15143

Synergistic effect of modified anhydrous magnesium carbonate and hexaphenoxycyclotriphosphazene on flame retardancy of ethylene-vinyl acetate copolymer

Yuan Liu,[a] Shiai Xu, *[ab] Qinghua Chen,[a] Jie Xu[a] and Beibei Sun[b]

Ethylene-vinyl acetate copolymer (EVA) is widely used in various applications; however, its flammability limits its application in wire and cable industries. In this study, 3-methacryloxypropyltrimethoxysilane (KH570) was successfully grafted onto the surface of anhydrous magnesium carbonate (AMC) by alkali activation treatment. The KH570 modified AMC (AMC@KH570) was then introduced into the EVA matrix along with hexaphenoxycyclotriphosphazene (HPCTP) to assess their effects on the flame retardancy and mechanical properties of EVA composites. The results illustrate a significant synergistic effect in enhancing the flame retardancy of EVA composites by using AMC@KH570 and HPCTP, and the limiting oxygen index (LOI) and vertical burning test (UL-94) of EVA filled with 5 wt% HPCTP and 45 wt% AMC@KH570 (mAMC/H-45-5) reached 27.6% and V-0, respectively. The flame retardant mechanism was investigated by thermogravimetric/infrared (TG-IR) spectroscopy and residual carbon composition analysis. The results show that the thermal decomposition of AMC@KH570 and HPCTP consists of gas dilution, free radical quenching, and catalytic carbonization. Furthermore, KH570 works as a bridge to improve the compatibility of AMC and EVA matrix, which offsets the mechanical loss of EVA to some extent. The present research provides a new path to modify AMC and fabricate EVA composites with excellent flame retardant properties.

Received 4th March 2024
Accepted 30th April 2024

DOI: 10.1039/d4ra01669f

rsc.li/rsc-advances

1 Introduction

Ethylene-vinyl acetate copolymer (EVA), known for its excellent processing and molding capabilities, finds extensive application in the fields of foamed shoe materials, functional greenhouse films, and packaging films.[1–6] However, its inherent flammability restricts its application in electrical wires and cables, necessitating the enhancement of EVA flame retardancy.[7] Addition of flame retardants is a prevalent approach to augment the flame retardant performance of EVA.[5] Halogenated flame retardants are susceptible to migration and bioaccumulation, frequently leading to generating numerous toxic gases and smoke during combustion. Therefore, in recent years, researchers have focused primarily on developing halogen-free flame retardants (HRRs) characterized by being cost-effective, non-toxic, and non-dripping.[5,8] These include phosphorus-based flame retardants (*e.g.*, ammonium polyphosphate[9] and red phosphorus[6]), nitrogen-based flame retardants (*e.g.*, melamine cyanurate[10]), silicon-based flame retardants (*e.g.*, polyhedral oligomeric silsesquioxane[11]), and metal hydroxides (*e.g.*, magnesium hydroxide[5] and aluminum hydroxide[12]). Among these, anhydrous magnesium carbonate (AMC) is recognized as a competitive halogen-free flame retardant, offering advantages including a high decomposition temperature, rapid decomposition, and high thermal stability.[13–17] The notable heat absorption and CO_2 storage capacity of AMC contribute to its effectiveness in combustion processes. It releases CO_2 to dilute oxygen and flammable substances in the gas phase while producing magnesium oxide (MgO) in the condensed phase, hindering further heat/mass transfer.[15] In previous work, our team successfully prepared AMC using a simple method, demonstrating its excellent flame retardant and smoke suppression properties in PVC.[14,16,17] Due to the significant difference in surface properties between the inorganic flame retardant filler and the polymer matrix, and in order to achieve good flame retardancy, the filling amount of the inorganic filler usually exceeds 50 wt%, which will affect the mechanical properties of the composites. Therefore, it is necessary to improve the dispersion of inorganic powders in the matrix by surface modification, thus to increase the interfacial adhesion between the matrix and the filler.

Achieving high flame retardancy performance poses challenges when relying on a single flame retardant. Therefore,

[a]*School of Materials Science and Engineering, East China University of Science and Technology, Shanghai 200237, China. E-mail: saxu@ecust.edu.cn*
[b]*Qinghai Provincial Key Laboratory of Salt Lake Materials Chemical Engineering, School of Chemical Engineering, Qinghai University, Xining 810016, China*

a common approach is to integrate synergistic flame retardant fillers,[6] which include montmorillonite (MMT),[18] layered double hydroxides (LDHs),[19,20] zinc borate (ZB),[21,22] and alginate.[23] Despite their widespread use, these synergistic agents typically contain only one flame-retardant element, leading to reduced flame-retardant efficiency. Phosphonitrilic compounds, such as hexaphenoxycyclotriphosphazene (HPCTP), represent a hybrid class with alternating N and P elements, exhibiting excellent self-extinguishing properties during combustion.[24] HPCTP, possessing both phosphorus and benzene ring structures, demonstrates good thermal stability and flame retardancy.[25] Its application extends to various materials such as polyethylene (PE),[26] rigid polyurethane foam (RPUF),[27] and silicone rubber.[28] Shen *et al.*[26] utilized HPCTP as a coupling agent between ultra-high molecular weight polyethylene (UHMWPE) and magnesium hydroxide (MH) to enhance compatibility, resulting in an increase in LOI value from 21.5% to 24.5% with the addition of 25 phr of HPCTP. Furthermore, 25% improvement in the melt flow rate (MFR) was achieved after adding HPCTP. Zhang *et al.*[27] investigated the synergistic enhancement of flame retardancy in polyurethane foam by incorporating HPCTP and glass fiber, achieving an LOI of 28.7% with a 20 wt% addition of HPCTP, along with a Peak Heat Release Rate (PHRR) of only 162.22 kW m^{-2}, nearly one half of RPUF. Additionally, Zhang *et al.*[28] explored the combustion behavior of epoxy-modified vinyl silicone rubber (EMVSR) composite materials containing HPCTP, revealing that the pyrolysis products of HPCTP can react with EMVSR, forming silicon compounds containing P and N, which contribute to reinforcing and densifying the carbon layer, playing a crucial role in enhancing flame retardant performance.

This study aims to formulate a novel strategy to enhance the flame retardancy of EVA material. Laboratory-made anhydrous magnesium carbonate (AMC) was modified using KH570 containing ester groups. The modified and unmodified AMC along with HPCTP were incorporated into EVA matrix to investigate the thermal, mechanical, and flame-retardant properties of the resulting EVA composites. It is found that mAMC and HPCTP have a good synergistic flame retardant effect. Finally, the thermal degradation process and pyrolysis products of EVA composites were evaluated using TG-IR, X-ray photoelectron spectroscopy (XPS), and Raman spectroscopy. The present research can help to understand the flame retardant mechanism of the EVA/mAMC/HPCTP system and provide a reference for development of EVA composites with high flame retardancy.

2 Experiment

2.1 Materials

Ethylene-vinyl acetate copolymer (EVA 265, VA content, 28 wt%) was purchased from DuPont. AMC was prepared in our laboratory. Anhydrous ethanol, sodium hydroxide (NaOH), sodium carbonate (Na_2CO_3), KH570, and HPTCP were purchased from Titan Technology Co. Ltd. (Shanghai, China).

2.2 Preparation of samples

2.2.1 Synthesis of modified AMC. An alkaline treatment was applied to activate the AMC surface. The alkaline solution containing 1 mol L^{-1} NaOH and 0.1 mol L^{-1} Na_2CO_3 was added to a beaker, followed by 10 wt% AMC. The mixture was stirred at room temperature for 2 hours. Then, the obtained product was subjected to filtration by Buchner funnel suction and washed with anhydrous ethanol until the pH reached 7. The modified AMC denoted as OH-AMC, was dried at 100 °C for 24 hours. Subsequently, 3 wt% of KH570 was dissolved in a 95 vol% ethanol solution, and subjected to ultrasonic hydrolysis for 20 minutes. The solution was poured into a single-necked flask containing OH-AMC and stirred magnetically at 80 °C for 4 hours. The resulting product (AMC@KH570) was filtered, washed, and dried in a 60 °C oven for 12 hours.

2.2.2 Preparation of EVA composites. EVA, AMC, AMC@KH570, and HPCTP were dried at 50 °C for 10 hours before processing. The components were blended in a torque rheometer (Rheocord 300P, Haake, Karlsruhe, Germany) at 60 rpm for 10 minutes at 170 °C. The resulting mixture was pressed to form thin sheet samples measuring 2 mm and 3 mm in thickness. Details of the samples in this experiment are listed in Table 1.

2.3 Characterization

The samples were analyzed for physical phase and crystal structure using an Ultima IV X-ray diffractometer (XRD, Rigaku, Japan). The scanning was operated at a rate of 4° min^{-1} within 10° to 80°. Surface functional groups were analyzed using an FTIR spectrometer (NICOLET 6700). Surface morphology was observed using an S-4800 field emission scanning electron microscope (SEM, Hitachi, Japan). LOI values were determined according to ASTM D2863-2000 using a JF-5 Oxygen Index Meter (Nanjing Yixuan Instrument and Equipment Co., Ltd., China). The UL-94 test was conducted

Table 1 The formulations of EVA composites

Sample	EVA (wt%)	AMC (wt%)	AMC@KH570 (wt%)	HPCTP (wt%)	LOI (%)	UL-94
EVA	100	—	—	—	18.6	No rating
H-5	95	—	—	5	22.3	No rating
AMC-50	50	50	—	—	22.2	No rating
mAMC-50	50	—	50	—	24.5	V-2
AMC/H-45-5	50	45	—	5	24.4	V-2
mAMC/H-45-5	50	—	45	5	27.6	V-0
mAMC/H-40-10	50	—	40	10	27.9	V-0

using the CZF-3 Vertical Flammability Tester (Dongguan Aolan Test Equipment Co., Ltd., Dongguan, China) by ASTM Standard D2863-17. Cone calorimeter tests (Stanton Redcroft, UK) were performed according to ISO 5660 standard procedures by a cone calorimeter (Kunshan Modisco Combustion Technology Instrument Co., Ltd., China) at a heat flux of 35 kW m^{-2}.

3 Results and discussion

3.1 Characterization of AMC, OH-AMC and AMC@KH570

The XRD patterns of standard $MgCO_3$ (PDF#99-0027),[14,17] standard $Mg(OH)_2$ (PDF#99-0021),[17] AMC, OH-AMC and AMC@KH570 are shown in Fig. 1a. A comparison between AMC and PDF#99-0027 illustrates the successful synthesis of crystalline particles in AMC with remarkably high characteristic peak intensity, indicating excellent crystallinity. In OH-AMC, the characteristic peak of AMC is present, alongside characteristic peaks of $Mg(OH)_2$ (PDF#99-0021) corresponding to crystal planes ((001), (100), (011), (012), (110), (111), (103), and (201)). This observation suggests the formation of a $Mg(OH)_2$ layer on the surface of AMC after alkali treatment. In AMC@KH570, no new characteristic peaks are observed. However, the intensity of characteristic peaks is weaker, indicating that KH570 does not alter the crystal structure of OH-AMC. Instead, a layer of KH570 is deposited on the surface of OH-AMC, leading to a reduction in characteristic peak intensity. The XRD results confirm the successful alkali treatment of AMC and the grafting of KH570 onto the surface of OH-AMC.

The chemical structures of AMC, OH-AMC, and AMC@KH570 were analyzed using FTIR (Fig. 1b). The peaks observed at 747 and 885 cm^{-1} denote in-plane and out-of-plane bending vibrations of CO_3^{2-}, respectively. Moreover, the peak at 1434 cm^{-1} corresponds to the asymmetric stretching vibration of C–O,[15,29] indicating characteristic features of AMC crystals. Additionally, the peak at 3442 cm^{-1} corresponds to the stretching vibration of O–H (hydroxyl or carboxyl), indicating the presence of hydroxyl and carboxyl groups on the surface of AMC particles.[14,16,30] After alkali treatment, OH-AMC exhibits a strong hydroxyl peak at 3698 cm^{-1}, indicating an increased content of hydroxyl groups on the surface of AMC. These hydroxyl groups provide more active sites for the subsequent grafting of silane coupling agents. In AMC@KH570, the peaks corresponding to C–O and CO_3^{2-} remain unchanged, while the absorption peak of Si–O–Mg appears at 1627 cm^{-1},[31] suggesting successful grafting of KH570 onto the surface of AMC.

The morphologies of AMC, OH-AMC, and AMC@KH570 were characterized using SEM. Fig. 2a uniformly sized cubic-shaped particles of AMC, with an approximate diameter of 10 μm, were successfully prepared. Alkaline treatment hardly changes the particle size and cubic morphology of AMC, while the surface of OH-AMC becomes rougher (refer to Fig. 2b). Hexagonal crystals of $Mg(OH)_2$ are evident on the surface of AMC, indicating successful alkaline treatment. In Fig. 2c, AMC@KH570 exhibits a surface morphology similar to OH-AMC, albeit with a blurred outline of $Mg(OH)_2$, possibly due to a thin layer of KH570.

The TGA and DTA curves for AMC and HPCTP are shown in Fig. 3a and b. The initial decomposition temperature (T_5) and the fastest decomposition temperature (T_{rpd}) of the materials are summarized in Table 2. HPCTP shows the lowest T_5 at 350 °C, leaving only 1.1% residue after pyrolysis. AMC exhibits only one thermal weight loss process, which is the overflow of CO_2 in AMC molecules. The T_{rpd} of AMC aligns with that reported in the literature,[14,16] resulting in a MgO residue of 50.6%. AMC@KH570 exhibits two thermal decomposition processes, with a T_5 of 369.3 °C lower than AMC, due to the decomposition of KH570 on the surface. Additionally, the T_{max} peak of AMC@KH570 is lower than AMC, indicating higher thermal stability in AMC@KH570. The residue mass of AMC is 1.6 wt%

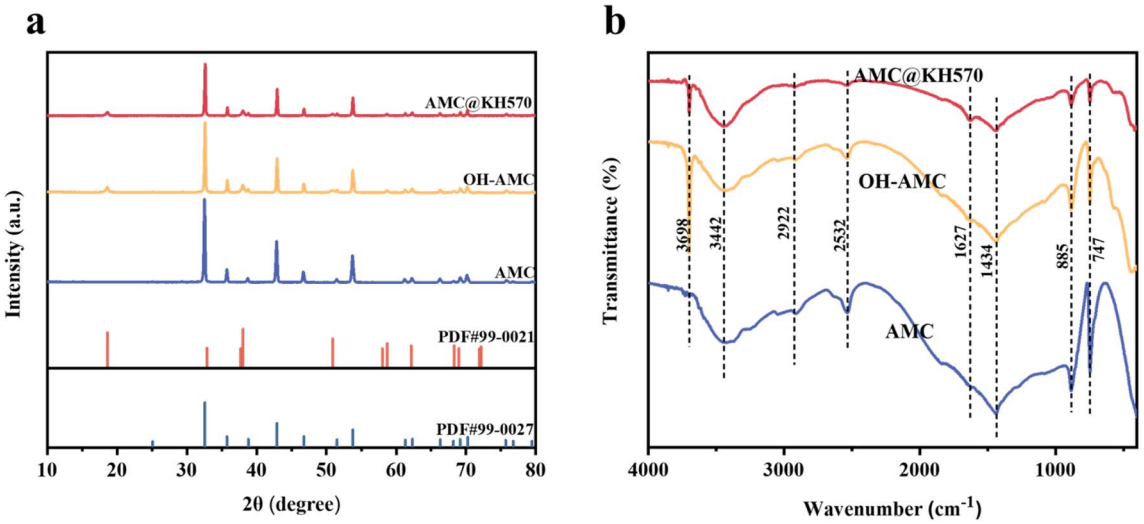

Fig. 1 XRD patterns (a) and FTIR spectra (b) of AMC, OH-AMC, and AMC@KH570.

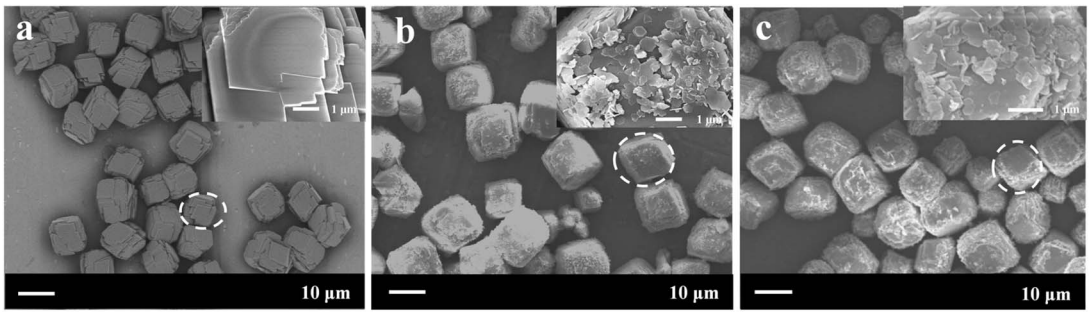

Fig. 2 SEM images of (a) AMC, (b) OH-AMC, and (c) AMC@KH570.

higher than AMC@KH570, indicating that the content of KH570 on the surface of AMC@KH570 is about 1.6 wt%.

3.2 Mechanical property

The mechanical properties of pure EVA and EVA composites were evaluated by tensile tests, as shown in Fig. 4. Pure EVA displays a fracture tensile strength (TS) of 12.4 MPa and an elongation at break (EB) of 1379%. EVA composite materials containing 5 wt% HPCTP exhibit optimal mechanical properties, with TS and EB values of 15.0 MPa and 1520.1%, respectively. This is attributed to the well-dispersed HPCTP in EVA, reinforcing the EVA matrix. Incorporating AMC@KH570, in an equivalent proportion to AMC, enhances both the TS and EB of the EVA composite. Specifically, compared to AMC-50, mAMC-50 demonstrates a 50% increase in TS and a 7% increase in EB. Similarly, in comparison to AMC/H-45-5, mAMC/H-45-5 achieves a 17% rise in TS and a 14% increase in EB. This is attributed to the strengthened interfacial interaction between AMC and the EVA matrix by KH570 modification. Comparing mAMC/H-45-5 with mAMC/H-40-10, it can be observed that increasing HTCTP content reduces the TS of EVA composite materials. Therefore, an optimal ratio of 9 : 1 between AMC and HPCTP is determined, while excess HPCTP may lead to potential aggregation, resulting in decreased EB and TS. This observation aligns with the results reported by other researchers.[26,28]

Table 2 TGA data of AMC, AMC@KH570, and HPCTP under N_2

Samples	T_5 (°C)	R_{rpd}/T_{rpd} (% min^{-1} $°C^{-1}$)	Residue content (%)
AMC	527.3	14.8/568.5	50.6
AMC@KH570	369.3	12.0/554.5	49.0
HPCTP	350.8	280.0/428.5	1.1

3.3 Dispersion of flame retardant in EVA matrix

Strong adhesion and effective dispersion between the filler particles and the polymer matrix are crucial for enhancing the mechanical properties of composite materials. As shown in Fig. 5, the dispersion of AMC, AMC@KH570, and HPCTP in the EVA matrix was characterized by the morphologies of the cryo-fractured surfaces of EVA composites after quenching in liquid nitrogen. In Fig. 5a, the fracture surface of pure EVA exhibits a very smooth morphology, whereas fracture surfaces of AMC-50 (Fig. 5b) and AMC/H-45-5 (Fig. 5d) appear rough and distinct, indicating inadequate interfacial interaction with the EVA matrix. In contrast, the fracture surfaces of

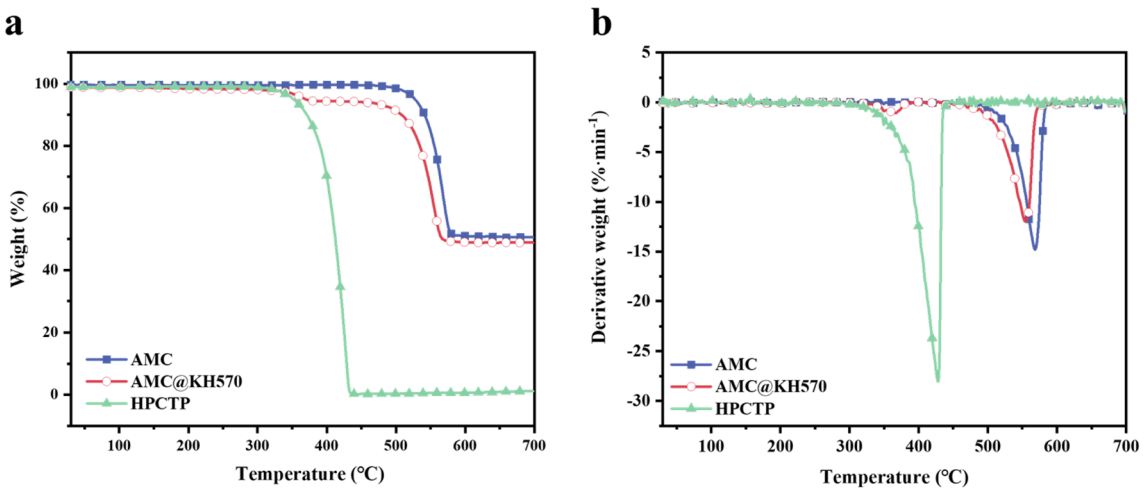

Fig. 3 TG (a) and DTG (b) curves of AMC, AMC@KH570, and HPCTP at a heating rate of 10 °C min under N_2 atmosphere.

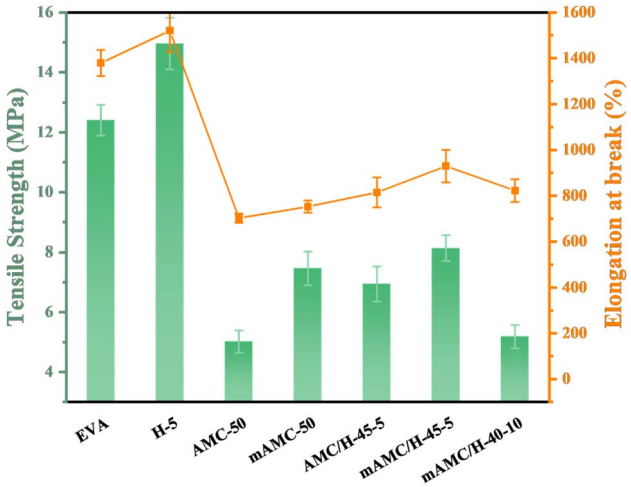

Fig. 4 Mechanical properties of EVA and its composites.

mAMC-50 (Fig. 5c) and mAMC/H-45-5 (Fig. 5e) become smoother, with a blurred boundary between AMC@KH570 and the EVA matrix. AMC@KH570 is uniformly distributed into the EVA matrix, further confirming the enhanced interfacial interaction between AMC@KH570 and EVA. This may be due to the ester group structure in the KH570 molecule, similar to that of the EVA matrix. Consequently, EVA composites containing AMC@KH570 exhibit superior mechanical properties under identical conditions. A comparison between mAMC/H-45-5 (Fig. 5e) and mAMC/H-40-10 (Fig. 5f) reveals aggregation occurrence in the EVA composite material as the HPCTP content increases (highlighted by the red area in Fig. 5f), leading to mechanical property deterioration in mAMC/H-40-10. As can be seen from Fig. 5g, when the HPCTP content is 5 wt%, HPCTP can be homogeneously dispersed in the EVA matrix without obvious aggregation.

3.4 Thermal stability of EVA composites

TGA tests were used to evaluate the decomposition behavior and carbonization ability of EVA, AMC-50, mAMC-50, and mAMC/H-45-5 composites, as depicted in Fig. 6 and Table 3. Pure EVA with a T_{intial} of 331.6 °C, exhibits minimal residual char at 700 °C and undergoes two distinct decomposition stages. The first peak, observed at 350.1 °C, exhibits a maximum degradation rate of 4.0% min^{-1}, primarily due to vinyl acetate decomposition and the formation of an unsaturated polyene structure resulting from the transformation of acetic acid groups in side chains into the gaseous state.[32] At 468.6 °C, the main process involves the fracture of the main unsaturated chains and the volatilization of residual carbon, with polyene thermally decomposing into alkyl during the second peak, showing a maximum degradation rate of 21.6% min^{-1}.[33,34] Upon the addition of AMC and AMC@KH570, the thermal decomposition exhibits three stages, raising $T_{initial}$ to 344.8 and 341.8 °C, respectively. The substantial reduction in the maximum degradation rate suggests improved thermal stability, with AMC effectively inhibiting polyene decomposition. In the third stage, the primary process is CO_2 decomposition in AMC. Replacing AMC@KH570 with 5 wt% of HPCTP, the $T_{initial}$ is reduced to 334.6 °C compared to mAMC-50, which is still slightly higher than 331.6 °C of pure EVA. This

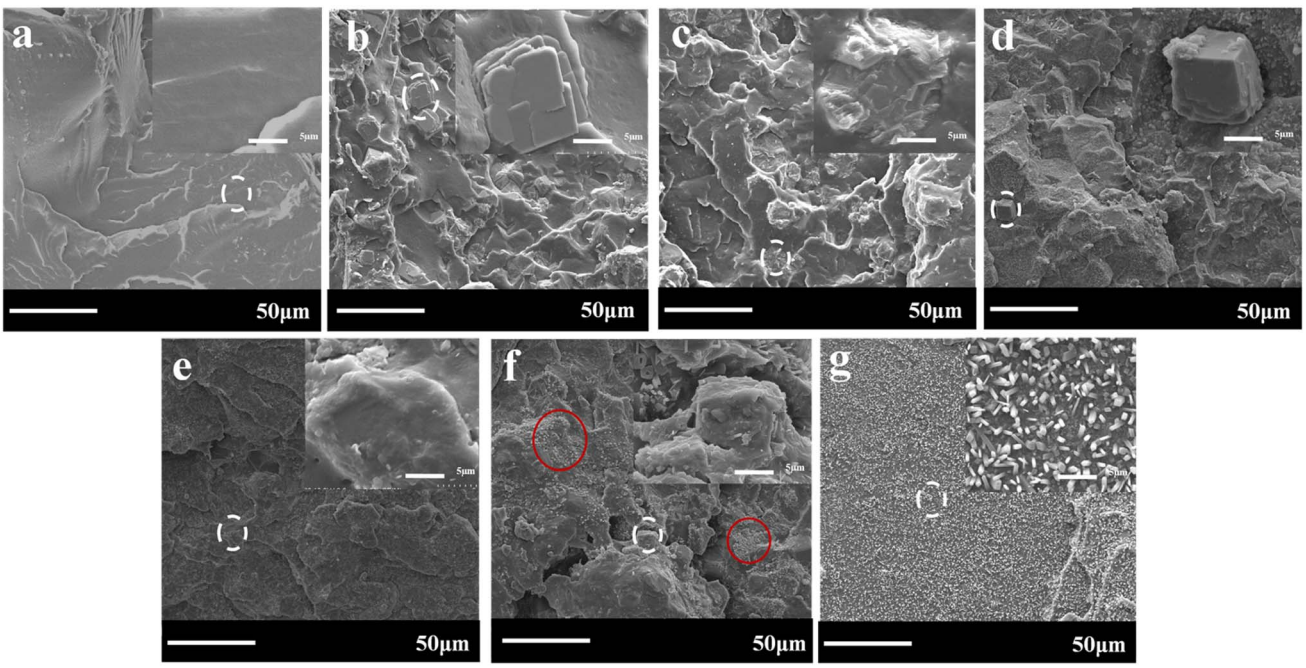

Fig. 5 SEM micrographs of EVA and EVA composites: (a) EVA, (b) AMC-50, (c) mAMC-50, (d) AMC/H-45-5, (e) mAMC/H-45-5, (f) mAMC/H-40-10, and (g) H-5.

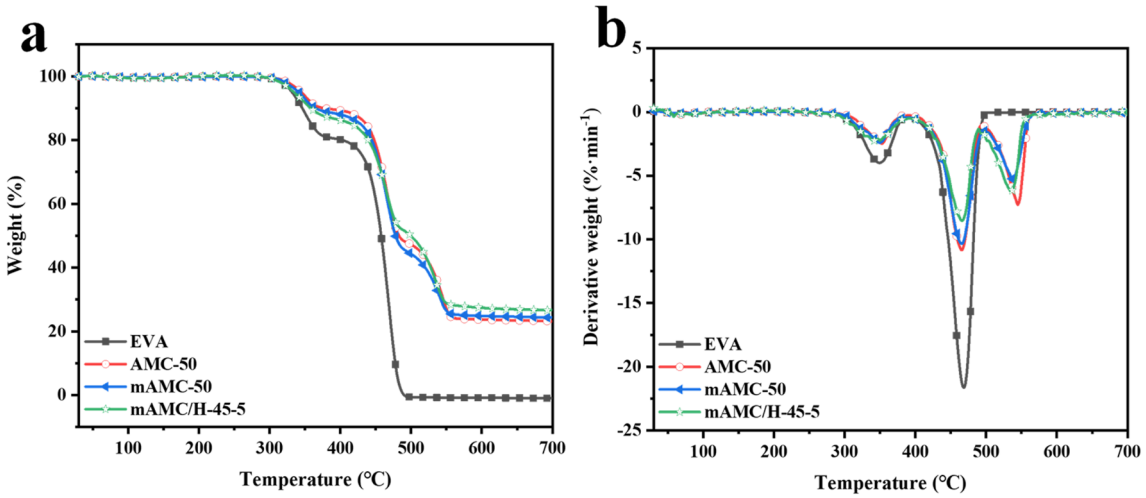

Fig. 6 TG (a) and DTG (b) curves of EVA, AMC-50, mAMC-50, and mAMC/H-45-5 at a heating rate of 10 °C min^{-1} under N_2 atmosphere.

Table 3 TGA data of EVA and EVA composites under N_2

Samples	$T_{initial}$ (°C)	R_{max1}/T_{peak1} (% min^{-1} °C^{-1})	R_{max2}/T_{peak2} (% min^{-1} °C^{-1})	R_{max3}/T_{peak3} (% min^{-1} °C^{-1})	Residue content (%)
EVA	331.6	4.0/350.1	21.6/468.6	—	0
AMC-50	344.8	2.5/353.5	10.8/465.9	7.1/546.0	23.3
mAMC-50	341.8	2.4/350.1	10.3/466.1	5.2/538.6	24.4
mAMC/H-45-5	334.6	2.2/342.0	8.4/467.2	6.2/536.3	26.6

phenomenon may be due to HPCTP decomposition at low temperatures. HPCTP degradation contributes to dense residual carbon formation, protecting the sample from further degradation. Among 50 wt% loaded materials, mAMC/H-45-5 with the highest residue content (26.6%) results from incorporating both HPCTP and AMC@KH570, indicating a synergistic effect between them.

3.5 Flame retardancy of EVA composites

The flame retardancies of pure EVA and EVA composites were evaluated using LOI and UL-94 ratings, and the results are summarized in Table 1. Pure EVA exhibits a relatively low LOI value of 18.6%, failing the UL-94 test as it consistently drips after ignition, burning for over 60 seconds and reaching the fixture, indicative of its high flammability. The LOI value of

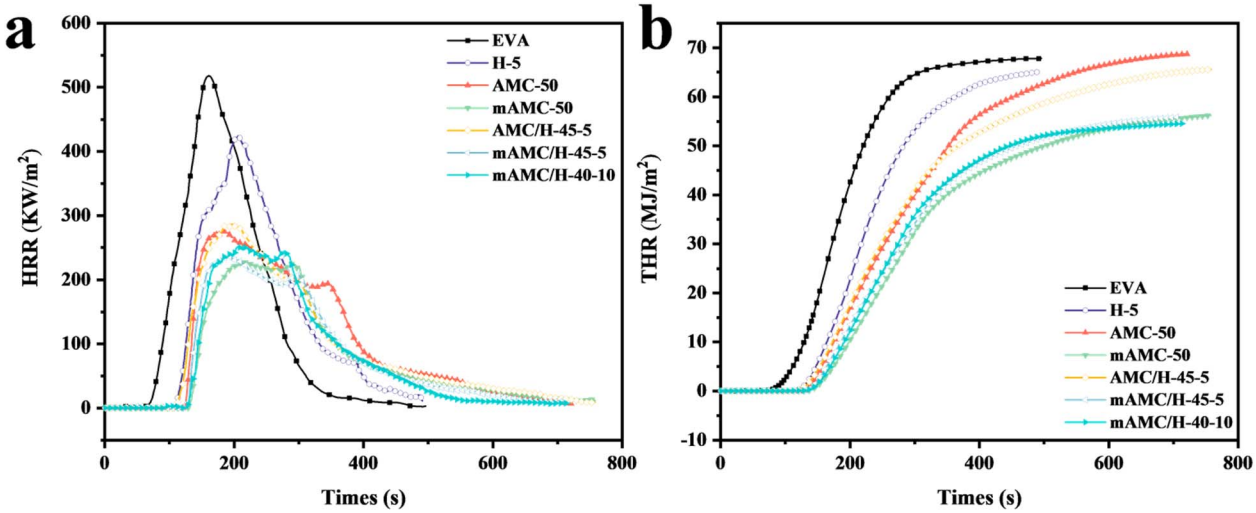

Fig. 7 HRR (a) and THR (b) curves of neat EVA and EVA composite.

AMC-50 slightly increases to 22.2%. Compared with AMC-50, LOI values of mAMC-50 and AMC/H-45-5 are increased by 2.3% and 2.2% respectively, passing UL-94 V-2 rating. This indicates that KH570 modified AMC or partially replacing AMC with HPCTP can further enhance the flame-retardant properties of EVA composite materials. The breaking of Si–O bonds in the silane coupling agent on the surface of AMC@KH570 alters the thermal degradation pathway, improving the overall flame retardancy. Additionally, the incorporation of HPCTP contributes to the formation of a more stable char layer. LOI values of mAMC/H-45-5 and mAMC/H-40-10 reach 27.6% and 27.9%, respectively, passing UL-94 V-0 ratings. These results indicate a synergistic flame-retardant effect between AMC@KH570 and HPCTP in EVA blends.

CCT analysis was employed to investigate the combustion behavior of pure EVA and EVA composite materials in a real fire scenario. The corresponding Heat Release Rate (HRR) and Total Heat Release (THR) are depicted in Fig. 7. Ignition Time (TTI), Peak Heat Release Rate (PHRR), Peak Heat Release Time (T_{PHRR}), and Total Heat Release (THR) are collected in Table 4. Pure EVA exhibits a short TTI, indicating rapid combustion. The PHRR (517.9 kW m^{-2}) of pure EVA is higher than that of other samples, signifying a heightened fire hazard. Incorporating HPCTP into EVA matrix reduces the PHRR of H-5 to 424.4 kW m^{-2}, decreased by 18.1% compared to pure EVA. Notably, the HRR for all AMC-containing EVA composites significantly decreases. Specifically, compared to pure EVA, the PHRR of AMC-50, mAMC-50, AMC/H-45-5, mAMC/H-45-5, and mAMC/H-40-10 decreases to 275.6, 223.7, 286.4, 237.7 and 249.2 kW m^{-2}, respectively, reduced by 46.8%, 56.8%, 44.7%, 54.1% and 51.9%, respectively. Moreover, the THR of all EVA composites except AMC-50 is lower than pure EVA (Fig. 7b), indicating flame retardant efficiency in reducing heat diffusion. Additionally, samples featuring AMC@KH570 exhibit more pronounced reductions, suggesting the role of KH570 in suppressing heat diffusion.

Table 4 Cone calorimeter data of neat EVA and EVA composite

Sample	TTI (s)	PHRR (kW m^{-2})	T_{PHRR} (s)	THR (MJ m^{-2})
EVA	63	517.9	161	67.8
H-5	129	424.4	227	65.0
AMC-50	124	275.6	183	68.7
mAMC-50	129	223.7	219	56.2
AMC/H-45-5	110	286.4	196	65.6
mAMC/H-45-5	127	237.7	191	55.9
mAMC/H-40-10	126	249.2	208	54.6

3.6 Residual carbon morphology

The charred layer is considered to have a significant influence on the flame retardancy. Digital photographs depicting the residue after the CCT combustion test are presented in Fig. 8. Pure EVA exhibits minimal residue (Fig. 8a), while H-5 (Fig. 8b) retains a small amount of charred flakes. Samples containing AMC exhibit a higher amount of residue, consistent with the results of TGA testing. The carbon layer of AMC-50 is fragmentary and not continuous, leading to the phenomenon of fly ash. The char layers of AMC/H-50 (Fig. 8d) and mAMC-50 (Fig. 8e) are continuous but relatively loose, with some small holes on the surface. Conversely, the char layers of mAMC/H-45-5 (Fig. 8f) and mAMC/H-40-10 (Fig. 8g) are denser and more continuous, featuring smoother surfaces. The denser char layer reduces volatile release, thus mitigating erosion of underlying materials by heat and oxygen from pores and cracks.

SEM analysis was employed to further examine the morphology of the charred layer post-CCT, confirming the flame retardant mechanism. Fig. 9a displays evident AMC-50 fragments, hindering the formation of a dense barrier on the polymer surface. Both mAMC-50 (Fig. 9b) and AMC/H-45-5 (Fig. 9c) exhibit continuous residual carbon, although some

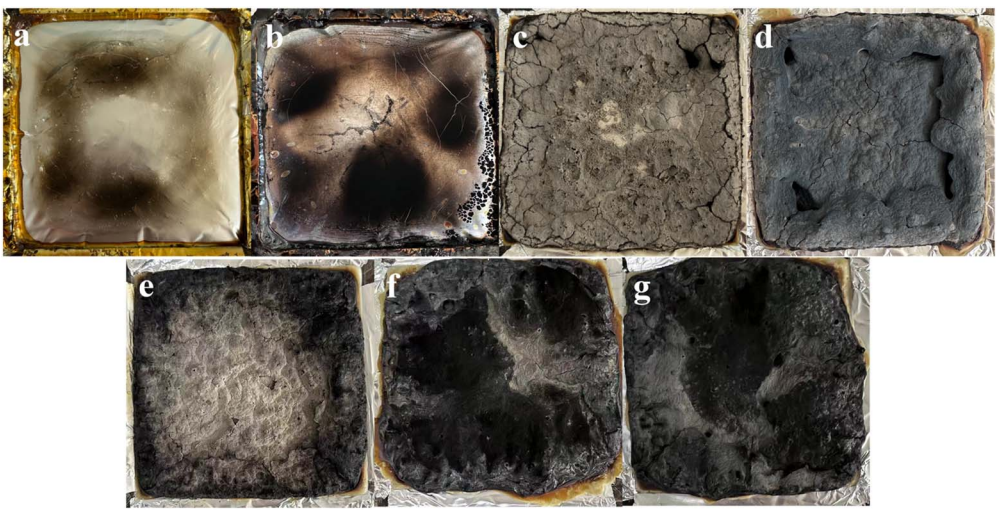

Fig. 8 The digital photos of char residues after cone calorimeter test: (a) EVA, (b) H-5, (c) AMC-50, (d) mAMC-50, (e) AMC/H-45-5, (f) mAMC/H-45-5, and (g) mAMC/H-40-10.

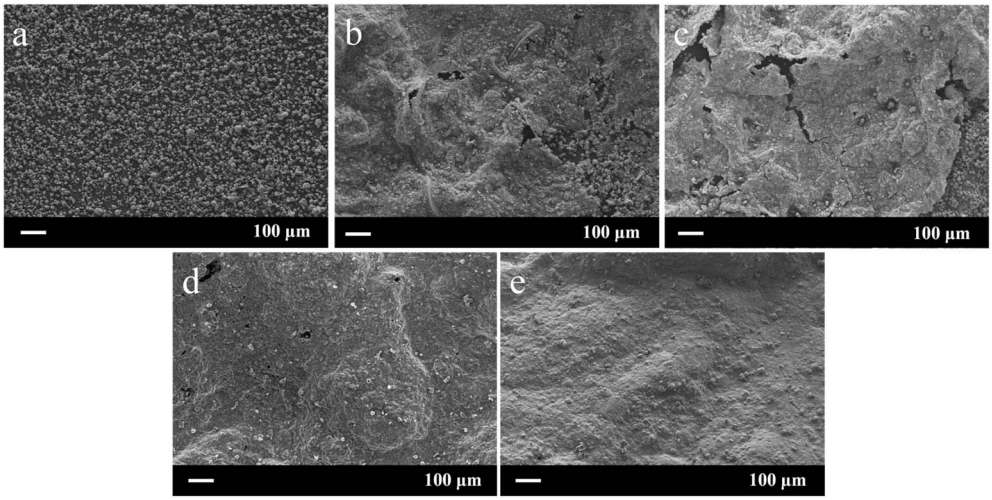

Fig. 9 SEM of char residues measured by CCT: (a) AMC-50, (b) mAMC-50, (c) AMC/H-45-5, (d) mAMC/H-45-5, and (e) mAMC/H-40-10.

remaining holes and cracks. The decomposition of KH570 and HPCTP generates a gelatinized substance adhering between AMC particles, resulting in a denser carbon layer, though the adhesion remains insufficient. As can be seen from Fig. 9d and e, the AMC particles are so tightly connected by the carbonization products of KH570 and HPCTP, with almost no visible cracks, which explains the best flame retardancy of mAMC/H-45-5 and mAMC/H-40-10.

The above observations further demonstrate the synergistic mechanism of AMC@KH570 and HPCTP. The pyrolysis products of HPCTP form a viscous colloid covering between the AMC particles. This enhances adhesion between AMC@KH570 particles and the EVA substrate, resulting in the formation of a dense charcoal layer that impedes the pyrolysis of EVA.

3.7 Flame retardant mechanism analysis

3.7.1 Vapor phase flame retardant. To further understand the synergistic flame-retardant mechanism between HPCTP and AMC@KH570, the gas-phase pyrolysis products of pure EVA, AMC-50, and mAMC/H-45-5 were analyzed using TG-IR. The 3D IR spectra of the composite are shown in Fig. 10(a, c and e), and the IR spectra of the gas-phase decomposition products at the corresponding temperatures are depicted in Fig. 10(b, d and f). In Fig. 10a and b, pure EVA reaches its initial decomposition peak at 350 °C. The absorption peaks at 1735 cm^{-1} (C═O), 1184 cm^{-1} (C–O), and 1364 cm^{-1} (C–H) can be attributed to the carboxyl groups (–COOH) generated by the removal of acetic acid molecules during the initial decomposition process of EVA.[7] As the temperature rises to 468 °C, the characteristic peaks of aliphatic hydrocarbons appear clearly at 2865 and 2935 cm^{-1}, indicating that the decomposition of polyolefins is the main concern at this stage. The peaks at 670 and 2358 cm^{-1} result from the removal of CO_2.[25,35] In Fig. 10c and d, the characteristic peaks related to CO_2 decomposition (670 and 2358 cm^{-1}) are significantly enhanced as the temperature increases to 546 °C. In Fig. 10e and f, observable characteristic peaks at 952, 1201, and 1364 cm^{-1} are derived from NH_3, P═O, and P–O–P,[36–38] respectively. These findings suggest that HPCTP in mAMC/H-45-5 initiates decomposition, producing phosphorus-containing radicals.[39]

3.7.2 Flame retardancy of condensed phases. To investigate the synergistic effect of AMC@KH570 and HPCTP on the graphitization structure and ordering degree of the carbon layer in EVA composites,[40] Raman spectra of the char residues of AMC-50 and mAMC/H-45-5 after CCT were determined. Two characteristic bands, the G band (1588 cm^{-1}) and the D band (1372 cm^{-1}) are observed in Fig. 11. The presence of G peaks indicates a graphitic structure within the char layer.[41] The degree of graphitization is determined by the ratio R ($R = I_D/I_G$),[41] with a value of 2.09 for AMC-50 and 2.33 for mAMC/H-45-5, suggesting higher graphitization in the latter. In conclusion, upon ignition, AMC@KH570 and HPCTP synergistically transform amorphous carbon into a graphite structure, thereby enhancing strength and densifying the carbon layer.

3.7.3 FTIR analysis of the char residue. The chemical structures and compositions of the carbon layers formed by AMC-50, mAMC-50, and mAMC/H-45-5 after CCT testing were analyzed using FTIR tests, and the results are shown in Fig. 12. The absorption bands at 3724, 3428, 1634, 1457, and 457 cm^{-1} are assigned to the asymmetric stretching vibration of O–H bond, stretching vibration of H_2O, bending vibration of H_2O, bending vibration of O–H bond and stretching vibration of Mg–

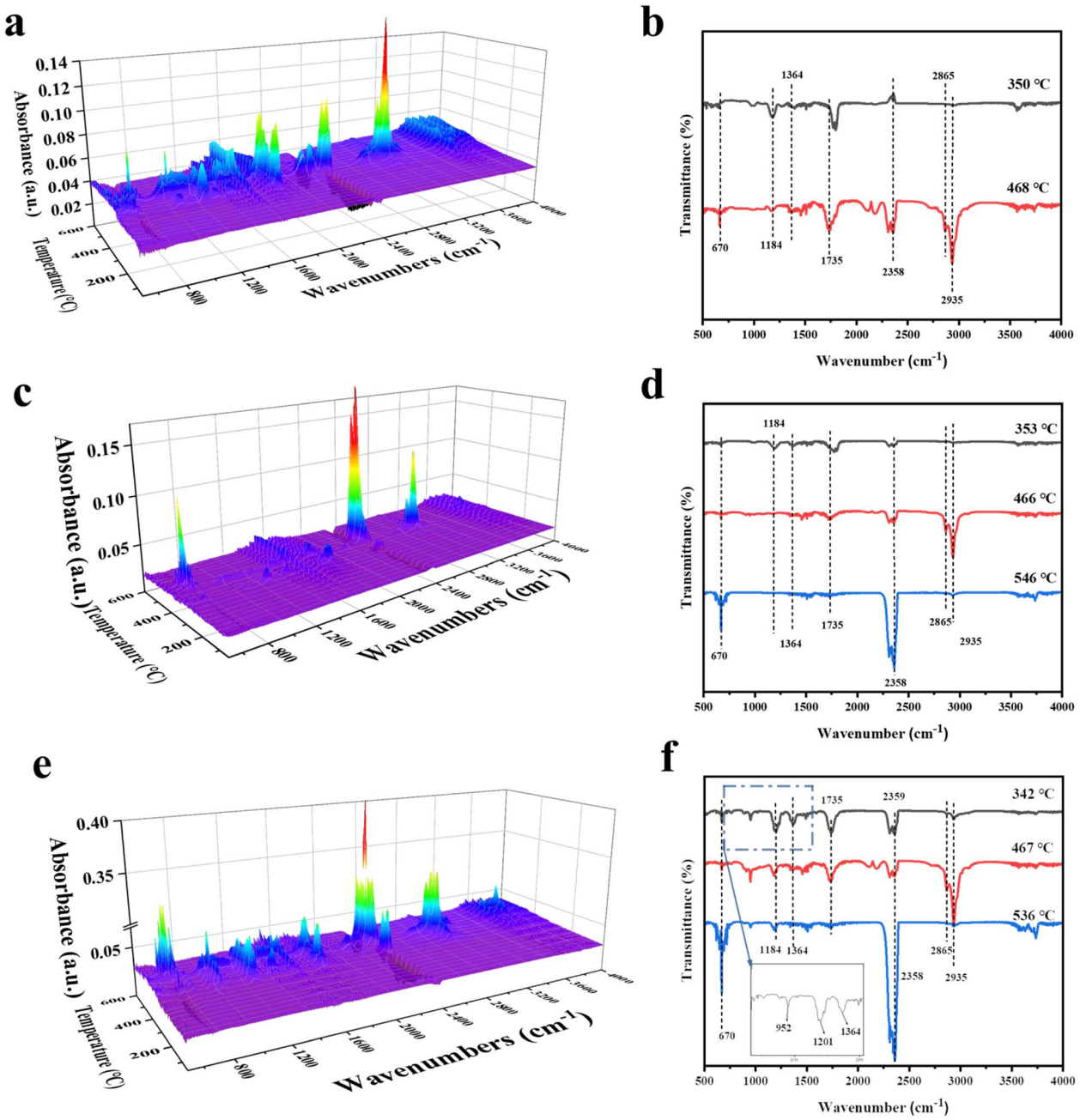

Fig. 10 3D TG-IR spectra of EVA (a), AMC-50 (c), mAMC/H-45-5 (e); FTIR spectra of pyrolysis products at different temperatures for EVA (b), AMC-50 (d), and mAMC/H-45-5 (f).

O bond. Peaks appearing at 2975, 2924 cm^{-1} correspond to the decomposition of EVA to produce $-CH_3$, $-CH_2$. The mAMC-50 shows a new absorption peak at 1120 cm^{-1}, which may be attributed to the stretching vibration of the Si–C bond. mAMC/H-45-5 in the band near 1264–938 cm^{-1} corresponds to the stretching vibration of the P–O–C. The above results indicate that the combination of HPCTP and KH570 with EVA forms a relatively stable Si–C and P–O–C carbon layer structure during combustion, elucidating the superior flame retardancy of mAMC/H-45-5.

A mechanistic model for the flame retardation of mAMC/H-45-5 composites was proposed, analyzing residues in both the gas phase (pyrolysis products) and coalesced phase (carbon residue) (Fig. 13). During the combustion of EVA composites,

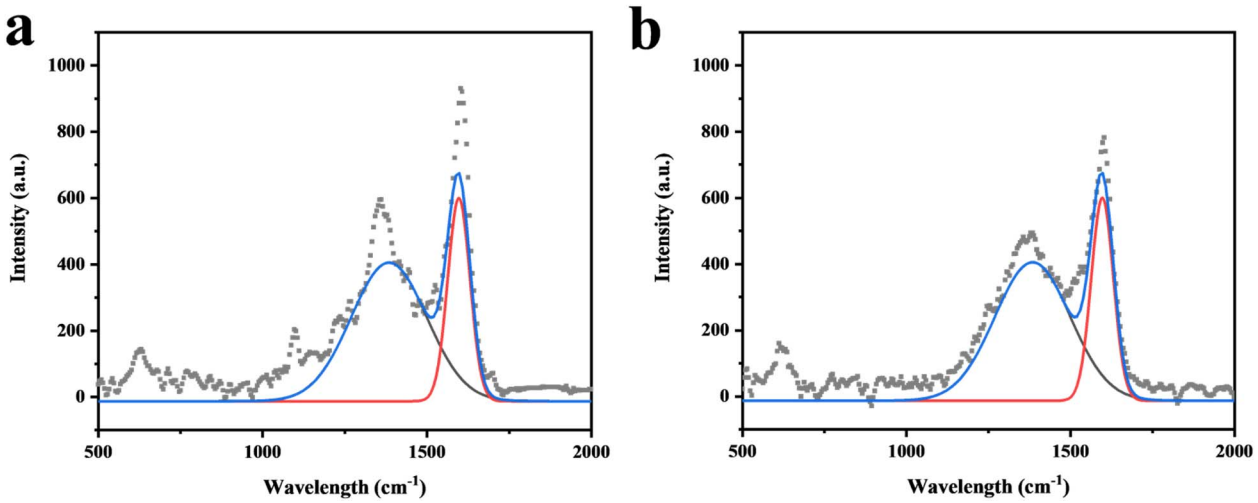

Fig. 11 Raman spectra of char residues: (a) AMC-50 and (b) mAMC/H-45-5.

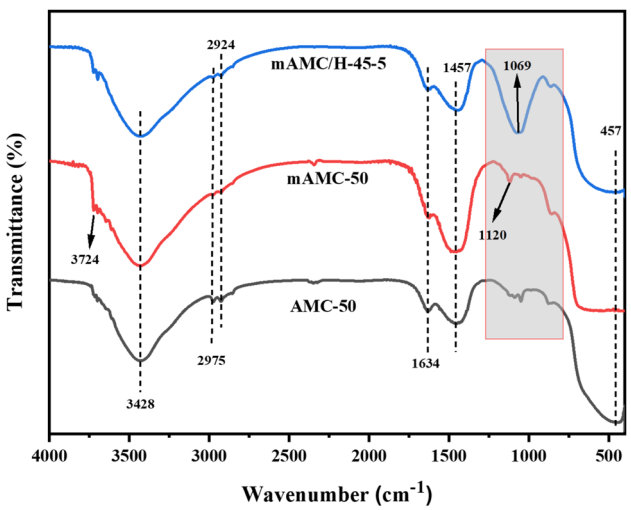

Fig. 12 FTIR spectra of char residues of AMC-50, mAMC-50 and mAMC/H-45-5.

HPCTP absorbs heat and decomposes, yielding PO·, PO_2·, phenoxy radicals, and NH_3, a non-flammable gas. Notably, PO·, PO_2·, and phenoxy radicals quench the H· and OH· generated by the combustion of EVA resin, hindering the radical chain reaction, with the resulting gelatinous substance bonding between AMC particles to form a dense carbonized layer, isolating oxygen and preventing further combustion. Additionally, NH_3 generated during combustion dilutes atmospheric oxygen. At low temperatures, the surface of KH570 undergoes exothermic decomposition, generating Si–O·, which reacts with carboxyl radicals released to form stable Si-containing compounds. At moderate temperatures, MH on the surface of AMC@KH570 can thermally decompose to produce H_2O, lowering the temperature and diluting the oxygen in the flame zone. In the high-temperature stage, AMC@KH570 absorbs heat, decomposing to generate MgO and CO_2. MgO covers the surface of the substrate to form a protective barrier. The denser CO_2 further insulates the flame zone from oxygen. In the gas phase, NH_3, H_2O, and CO_2 collectively dilute oxygen and the gaseous fuel. In the condensed phase, the generated MgO particles and a dense

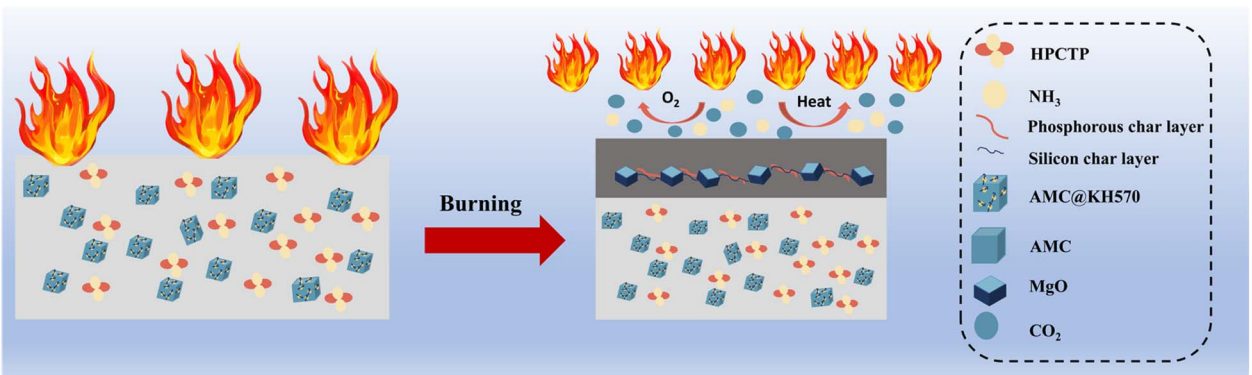

Fig. 13 Synergistic flame retardancy mechanism of the AMC@KH570/HPCTP mixture in EVA.

carbon layer containing P and Si cover the surface of the material, preventing the entry of oxygen and combustible gases, and insulating the heat source and fuel.

4 Conclusion

In this study, surface-modified AMC with KH570 was utilized to enhance its interfacial interaction with the EVA matrix and act as a synergist along with HPCTP to improve the flame retardancy of EVA. The results indicate that replacing AMC@KH570 with only 5 wt% HPCTP shows a significant flame retardant effect. Compared to pure EVA, the LOI value of mAMC/H-45-5 increases from 18.6% to 27.6%, achieving a V-0 rating in UL-94. THR decreases by 20.5%, and the TS and EB reach 8.1 MPa and 929.5%, respectively. Observing the morphological structure of char residues after CCT, conducted through digital cameras and SEM, confirms that the addition of AMC@KH570 and HPCTP can form a dense carbon layer on the material surface. TG-IR reveals the generation of inert gases (NH_3 and CO_2, *etc.*) in the gas phase to dilute O_2, heat, and combustible volatiles, thereby inhibiting combustion. Raman spectroscopy shows that HPCTP and KH570 can promote the formation of a dense graphite structure in the condensed phase, preventing further combustion of the material. This study introduces a novel strategy for applying AMC in enhancing EVA flame retardancy.

Conflicts of interest

There are no conflicts to declare.

Acknowledgements

This research is financially supported by the National Natural Science Foundation of China (U22A20434) and the Foundation from Qinghai Science and Technology Department (2023-ZJ-745).

References

1 C. Feng, M. Liang, W. Chen, J. Huang and H. Liu, *J. Anal. Appl. Pyrolysis*, 2015, **113**, 266–273.
2 T. F. A. Santos, G. C. Vasconcelos, W. A. de Souza, M. L. Costa and E. C. Botelho, *Mater. Des.*, 2015, **65**(1980–2015), 780–788.
3 C. Shi, X. Zou and P. Wang, *Constr. Build. Mater.*, 2018, **193**, 474–480.
4 K. Noor Saeed, A. Arbab Safeer, S. Luqman Ali, A. Latafat, F. Muhammad, S. Muhammad and K. Safaa I., *Z. fur Phys. Chem.*, 2019, **233**(9), 1233–1246.
5 S. Xu, Y. Han, C. Zhou, J. Li, L. Shen and H. Lin, *Chin. Chem. Lett.*, 2023, **34**, 107202.
6 J. Liu, Y. He, H. Chang, Y. Guo, H. Li and B. Pan, *Polym. Degrad. Stab.*, 2020, **171**, 109051.
7 H.-W. Di, C. Fan, H. He, N. Zhang, J.-L. Dong and Y.-T. Wang, *J. Therm. Anal. Calorim.*, 2023, **148**, 11717–11726.
8 B. W. Liu, H. B. Zhao and Y. Z. Wang, *Adv. Mater.*, 2022, **34**, 2107905.
9 J. Xu, Y. Niu, Z. Xie, F. Liang, F. Guo and J. Wu, *Chem. Eng. J.*, 2023, **451**, 138566.
10 J. J. Cheng, W. J. Qu and S. H. Sun, *Polym. Compos.*, 2019, **40**, E1006–E1014.
11 W. Zhang, X. Li and R. Yang, *Polym. Degrad. Stab.*, 2011, **96**, 2167–2173.
12 F. Hu, B. Cheng, K. Cong, D. Li, W. Zhang, Z. Qin and R. Yang, *Polymers*, 2023, **15**, 3312.
13 M. Hänchen, V. Prigiobbe, R. Baciocchi and M. Mazzotti, *Chem. Eng. Sci.*, 2008, **63**, 1012–1028.
14 Y. Lu, C. Zhao, S. Khanal and S. Xu, *Composites, Part A*, 2020, **135**, 105926.
15 Q. Bi, Y. Lu, C. Zhao, X. Ma, S. Khanal and S. Xu, *J. Appl. Polym. Sci.*, 2021, **138**, 51349.
16 C. Zhao, Y. Lu, X. Zhao, S. Khanal and S. Xu, *Polym.-Plast. Technol. Mater.*, 2021, **60**, 316–326.
17 K. Chai and S. Xu, *Adv. Powder Technol.*, 2022, **33**, 103776.
18 X. Wang, B. Bi, J. Liu, S. Yang, L. Zhou, L. Lu, Y. Wang, F. Xu and R. Huang, *J. Appl. Polym. Sci.*, 2018, **135**, 46361.
19 B. Guo, Y. Liu, Q. Zhang, F. Wang, Q. Wang, Y. Liu, J. Li and H. Yu, *ACS Appl. Mater. Interfaces*, 2017, **9**, 23039–23047.
20 Y. Liu, Y. Gao, Q. Wang and W. Lin, *Dalton Trans.*, 2018, **47**, 14827–14840.
21 W. Bartz, J. Kierczak, M. Gąsior and P. Wanat, *Archaeol. Anthropol. Sci.*, 2017, **9**, 279–291.
22 Y. Xu, R. Zhou, J. Mu, Y. Ding and J. Jiang, *Colloids Surf.*, 2022, **640**, 128400.
23 Y.-J. Xu, L.-Y. Qu, Y. Liu and P. Zhu, *Carbohydr. Polym.*, 2021, **260**, 117827.
24 W. Tan, L. Gao, J. Su, C. Zuo, Y. Ren and X. Liu, *Composites, Part A*, 2024, **177**, 107897.
25 Z. Wei, J. Wu, Z. Liu, Y. Gu, G. Luan, H. Sun, Q. Yu, S. Zhang and Z. Wang, *Polym. Adv. Technol.*, 2020, **31**, 1426–1436.
26 L. Shen, J. Li, H. Lin, S. Feng and Y. Zhang, *Polym. Bull. (Berlin)*, 2017, **74**, 3639–3655.
27 P. Zhang, D. Ma, J. Cheng, X. Zhang and X. Chen, *Polym. Compos.*, 2020, **41**, 3521–3527.
28 H. Zhang, J. Tian, L. Yan, S. Zhou, M. Liang and H. Zou, *Nanomaterials*, 2023, **13**, 563.
29 A. Grzechnik, P. Simon, P. Gillet and P. McMillan, *Phys. B*, 1999, **262**, 67–73.
30 M. Zheng, Y. Liu, K. Jiang, Y. Xiao and D. Yuan, *Carbon*, 2010, **48**, 1224–1233.
31 M. Yao, H. Wu, H. Liu, Z. Zhou, T. Wang, Y. Jiao and H. Qu, *Polym. Degrad. Stab.*, 2021, **183**, 109417.
32 A. G. Newton and K. D. Kwon, *Geochim. Cosmochim. Acta*, 2020, **291**, 92–109.
33 J. Wang, H. Shi, P. Zhu, Y. Wei and J. Hao, *Polymers*, 2020, **12**, 534.
34 J.-F. Li, W. Jiang and Y. Gao, *Polym. Degrad. Stab.*, 2023, **218**, 110570.
35 T. Cao, L. Yuan, A. Gu and G. Liang, *Polym. Degrad. Stab.*, 2015, **121**, 157–170.
36 L. Zhang, Y. Wang, Q. Liu and X. Cai, *J. Therm. Anal. Calorim.*, 2016, **123**, 1343–1350.

37 L. Long, J. Yin, W. He, Y. Xiang, S. Qin and J. Yu, *Polym. Compos.*, 2019, **40**, 1043–1052.
38 S. Wang, W. Wu, Q. Chen, Z. Ding, S. Li, A. Zhang, T. Tang, J. Liu and P. U. Okoye, *J. Appl. Polym. Sci.*, 2023, **140**, e53430.
39 B. Xu, W. Ma, X. Wu, L. Qian and S. Jiang, *Mater. Res. Express*, 2018, **5**, 045309.
40 L.-P. Dong, C. Deng and Y.-Z. Wang, *Polym. Degrad. Stab.*, 2017, **135**, 130–139.
41 B. Xu, W. Ma, X. Bi, L. Shao and L. Qian, *J. Polym. Environ.*, 2019, **27**, 1127–1140.